中国激光

绿光泵浦的克尔透镜锁模翠绿宝石激光器

杨云霄[1,4]，于洋[2]，田文龙[1*]，朱江峰[1**]，魏志义[3]

[1]西安电子科技大学光电工程学院，陕西 西安 710071；

[2]西安电子科技大学前沿交叉研究院，陕西 西安 710071；

[3]中国科学院物理研究所北京凝聚态物理国家研究中心，北京 100190；

[4]航天江南集团有限公司，贵州 贵阳 550009

摘要 翠绿宝石激光器在医疗美容等领域发挥着重要的作用，其通常采用红光二极管(LD)激光器作为泵浦源，可以获得较高的转化效率，但红光LD激光器的光束质量较差，不适合直接作为克尔透镜锁模激光器的泵浦源，商用的绿光激光器以其优异的光束质量成为了克尔透镜锁模翠绿宝石激光器的首选泵浦源。报道了一种绿光泵浦的克尔透镜锁模翠绿宝石激光器。实验采用商用532 nm全固态绿光激光器作为翠绿宝石激光器的泵浦源，当泵浦光功率为10 W时，实现了稳定的锁模脉冲输出，重复频率为92 MHz，平均功率为369 mW，脉冲宽度为86 fs，中心波长为749 nm，光谱半峰全宽为6.3 nm。

关键词 激光器；全固态激光器；绿光泵浦；克尔透镜锁模；翠绿宝石

中图分类号 TN248.1 **文献标志码** A **DOI**：10.3788/CJL230641

1 引 言

超短脉冲激光器在工业加工[1-2]、医疗治疗与诊断[3]、通信探测[4]等领域有着广泛的应用。其中，700～900 nm波段飞秒激光光源是双子荧光探测的理想光源，该波段激光发出的荧光探针能穿透更深层的生物组织，降低光对组织结构的损伤与生物组织自荧光的影响，这在组织细胞等微小结构的病症诊断治疗方面有极大的应用潜力[5]。此外，该波段激光器还可以应用于超快光谱[6]、频率变换[7]和光学相干断层扫描[8]等方面。能产生该波段激光的增益介质除了Ti∶sapphire以外，还有部分掺Cr的晶体，如翠绿宝石(Cr∶$BeAl_2O_4$)、掺铬氟化铝锶锂(Cr∶LiSAF)、掺铬氟铝酸钙锂(Cr∶LiCAF)等。翠绿宝石晶体作为可调谐晶体之一，具有较宽的发射谱、良好的力学性能、高热导率和高损伤阈值，是较为优秀的激光增益介质。与Ti∶sapphire相比，它的受激发射截面(σ)只有0.7×10^{-20} cm^2，小了一个数量级，但其激光上能级寿命(τ)在室温下约为260 μs，因此$\sigma\tau$更大[9-10]，可以实现低阈值连续激光运转[11-12]。晶体优良的热力学性能、高热导率、高损伤阈值等优点使其能承受更高的泵浦功率[13]。翠绿宝石晶体又被称为亚历山大石。该晶体属于斜方晶系，是正双轴晶体，具有三个结晶轴，每个晶轴对应不同的偏振吸收谱。翠绿宝石晶体与钛宝石晶体一样都是可调谐的激光晶体，其光谱调谐范围为701～858 nm[14]。翠绿宝石晶体的吸收光谱覆盖400～700 nm波段，蓝光、绿光、黄光、红光波段的光源均可作为翠绿宝石激光器的泵浦源；发射光谱覆盖700～900 nm波段，该光谱宽度可以支持脉冲宽度小于20 fs的超短脉冲产生，在产生飞秒脉冲方面有着巨大潜力。

近年来，国内外关于翠绿宝石激光器的研究有很大进展，尤其是在锁模超快激光器方面。2016年，Ghanbari等[15]首次实现了脉冲宽度为170 fs的绿光泵浦翠绿宝石激光器的克尔透镜锁模(KLM)运转。2018年，该团队在上述研究基础上使用量子点半导体可饱和吸收镜(QD-SESAM)作为辅助启动锁模的元件，实现了脉冲宽度为380 fs的被动锁模输出[16]。2018年，Cihan等[17]使用多通腔克尔透镜锁模的方式获得了脉冲宽度为70 fs的实验结果。同年，该课题组利用相似的实验装置，以石墨烯作为可饱和吸收体，获得了翠绿宝石被动锁模实验结果，将脉冲宽度进一步压缩到65 fs[18]。2022年，研究者利用腔倒空主动锁模的方式获得了脉冲宽度为500 ps、单脉冲能量为100 mJ的多模脉冲输出，通过进一步调整腔长与模式匹配，在基模光输出状态下，获得了脉冲宽度小于300 ps、单脉冲能量为12.5 mJ的结果。2021年，Miao等[19]报道了

收稿日期：2023-03-23；**修回日期**：2023-04-23；**录用日期**：2023-06-19；**网络首发日期**：2023-06-29

基金项目：国家自然科学基金(11774277，62105253)、科技部国家重点研发计划(2017YFB0405202)、中央高校基本科研业务费(ZD2006，XJS222206)

通信作者：*wltian@xidian.edu.cn；**jfzhu@xidian.edu.cn

基于红光二极管(LD)泵浦的高重复频率自锁模翠绿宝石激光器,获得了重复频率为3.6 GHz、脉冲宽度为237 fs的锁模脉冲输出。而目前国内关于绿光泵浦的翠绿宝石锁模激光器的相关研究未见报道。绿光激光器以其优异的光束质量成为锁模光源的首选,虽然红光泵浦的翠绿宝石激光器可以获得更高的转化效率,但红光LD泵浦源的光束质量较差,不适合直接作为克尔透镜锁模激光器的泵浦源。商用的绿光泵浦源的光束质量好,可以直接作为克尔透镜锁模激光器的泵浦源,不需要对泵浦光进行复杂的整形,泵浦光源与产生的激光就能在晶体处实现较好的模式匹配,有利于克尔效应的产生,从而实现克尔透镜锁模。

在应用方面,翠绿宝石激光器被广泛地应用于医学美容。翠绿宝石激光器的出射波长通常在755 nm左右,该波段激光能更好地穿透皮肤的表皮层,到达真皮层,被毛囊中的黑色素吸收,有效地分解、祛除皮肤沉积的黑色素,被广泛用于激光脱毛、皮肤黑色素祛除等。目前,医美手术主要使用调Q翠绿宝石激光器的高脉冲能量熔解毛囊中的黑色素,但在过高的脉冲能量与较长的脉冲宽度的作用下,皮肤会产生泛红、过敏等现象。而翠绿宝石超快激光器可以有效地解决这一问题,更快更精准地作用于组织细胞,减少表皮细胞的损伤,降低术后皮肤泛红、过敏的概率[20-22];同时,锁模是获得超快激光尤其是飞秒激光较为经济、有效的途径之一。

基于上述应用研究背景,本文研究了绿光泵浦的克尔透镜翠绿宝石激光器,采用532 nm绿光激光器作为泵浦源,在10 W的泵浦功率下获得最大1.33 W的连续激光输出,对应转化效率为13.3%。进一步在腔内插入棱镜对,通过棱镜对补偿色散的方式实现了克尔透镜锁模运转,获得中心波长为749 nm、光谱半峰全宽(FWHM)为6.3 nm、平均功率为369 mW的锁模脉冲输出,输出脉冲宽度为86 fs,重复频率为92 MHz,单脉冲能量约为4.0 nJ,峰值功率约为46.5 kW。

2 实验设计

实验装置如图1所示。实验使用了通光长度为3 mm、掺杂物原子数分数为0.22 %的翠绿宝石晶体作为增益介质。由于泵浦光为线偏振光,以布儒斯特角对晶体通光面进行切割处理,一方面可以减小泵浦光与谐振腔内激光经过晶体的损耗,另一方面避免高功率泵浦损坏晶体表面镀膜。将晶体夹持在可通循环水的铜质热沉上,以水冷散热的方式缓解激光器工作时在晶体上的热积累,保持激光器的转化效率。

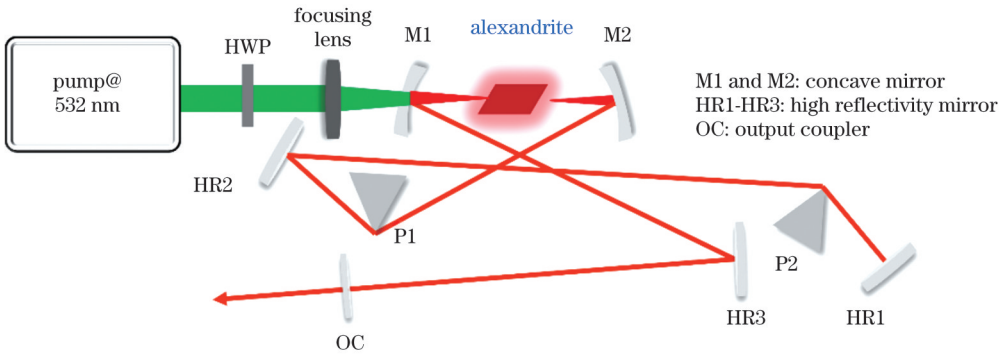

图1 绿光泵浦的翠绿宝石克尔透镜锁模激光器的实验装置示意图

Fig. 1 Schematic of experimental apparatus of KLM alexandrite laser pumped by green laser

泵浦源选用中心波长为532 nm、最高功率为10 W的激光器。泵浦光偏振态为S偏振态,故实验中加入一块半波片(HWP)对泵浦光的偏振态进行转换,使泵浦光偏振态与晶体b轴平行。泵浦光通过焦距(f)为100 mm的平凸透镜聚焦到晶体中心,在晶体中心位置处,泵浦光聚焦光斑直径约为27 μm,小于晶体中心位置处激光的束腰直径34 μm,并且晶体对泵浦光的吸收率为57.4%。谐振腔采用X形折叠腔,腔长约为1.62 m,对应的重复频率为92 MHz。其中M1与M2均为曲率半径为100 mm的双色凹面镜,对泵浦光高透,对激光高反。HR1、HR2和HR3均为620~1120 nm宽带镀膜平面高反镜。P1与P2是一对熔石英材质的等腰三棱镜,间距为620 mm,放置在谐振腔高反臂处,用于补偿腔内的正色散。输出耦合器的透射率分别为1%、2%和3%。翠绿宝石晶体的体积为4 mm×4 mm×3 mm。

3 实验结果与分析

实验中,我们首先使用不同透射率的耦合输出镜(OC)对连续光功率进行了测试,得到激光器在不同泵浦功率下的连续光输出功率曲线,如图2(a)所示。其中,当使用透射率为2%的耦合输出镜时,获得了最高功率为1.33 W的连续光(CW)输出,激光器出光阈值为0.37 W,对应转化斜效率(η)为14.3%;当使用透射率为1%与3%的耦合输出镜时,获得的最高连续光功率分别为918 mW和1.03 W,激光器出光阈值分别为0.42 W和2.38 W,对应斜效率分别为9.7%和14.4%。此时,使用光谱仪测量得到的连续光光谱如图2(b)所示,中心波长为750 nm。

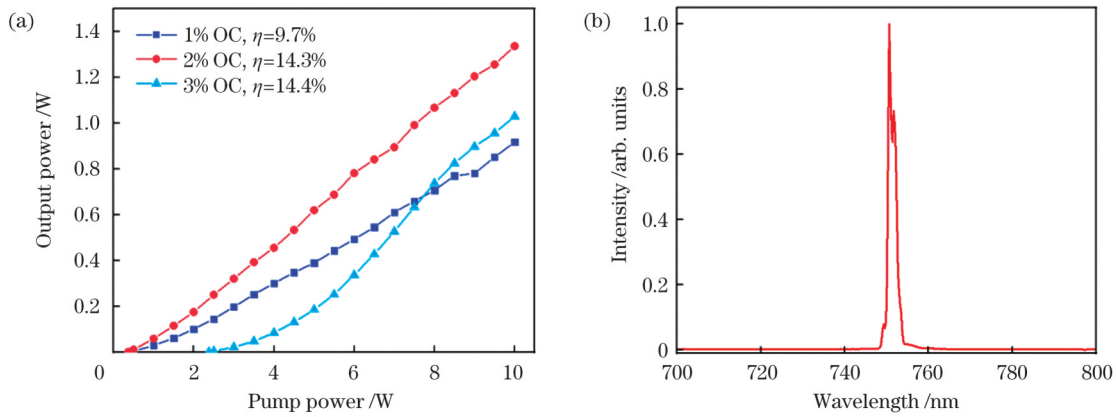

图 2　连续光实验结果。(a)连续光输出功率曲线;(b)连续光输出光谱

Fig. 2　Results of CW experiment. (a) CW output power curves; (b) CW output spectrum

进一步,我们利用透射率为 2% 的输出耦合镜进行了翠绿宝石激光器克尔透镜锁模实验研究。通过调节 M2 寻找合适的锁模位置,并适当改变三棱镜 P2 的插入量,引入扰动,在最高 10 W 泵浦功率下获得了 369 mW 的锁模脉冲输出。使用光谱仪测量了激光振荡器锁模后的光谱,测量结果如图 3(a)所示,锁模光谱中心波长为 748 nm,光谱 FWHM 为 6.3 nm。利用自相关仪对锁模脉冲的脉冲宽度进行了测量,假设脉冲为双曲正割型,得到锁模脉冲宽度为 105 fs,傅里叶变换后对应极限脉冲宽度为 93 fs,如图 3(b)所示;假设脉冲为洛伦兹型,拟合得到锁模脉冲宽度为 86 fs,对应极限脉冲宽度为 42 fs,如图 3(c)所示。图 4 为示波器中观测到的锁模脉冲序列,锁模状态较为稳定,对应重复频率为 92 MHz。

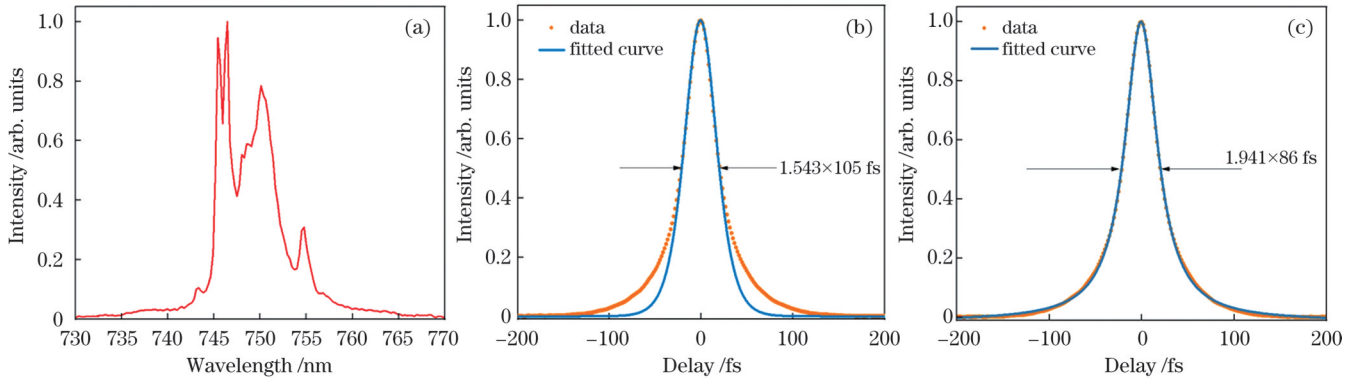

图 3　锁模实验结果。(a)锁模光谱图;(b)双曲正割函数拟合的自相关测量曲线图;(c)洛伦兹函数拟合的自相关测量曲线图

Fig. 3　Results of mode-locking experiment. (a) Measured mode-locking spectrum; (b) auto-correlation measurement curve fitted by hyperbolic secant function; (c) auto-correlation measurement curve fitted by Lorentz function

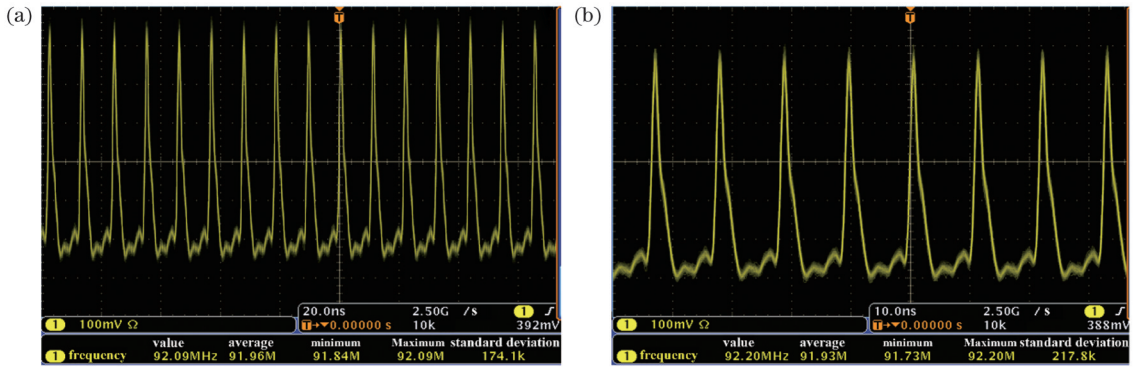

图 4　锁模脉冲序列。(a) 20 ns时间尺度;(b) 10 ns时间尺度

Fig. 4　Mode-locked pulse trains. (a) 20 ns time scale; (b) 10 ns time scale

根据测量得到的光谱结果进行傅里叶变换极限脉冲宽度计算,与测量拟合的脉冲宽度进行对比,结果表明,测量拟合的脉冲宽度与极限变换脉冲宽度有差距。该锁模状态说明振荡器输出的锁模脉冲带有一定量的

啁啾，限制了脉冲宽度的减小。实验获得的锁模光谱中心波长为748 nm，泵浦光入射偏振方向与b轴平行，通过Sellmeier方程计算得到该中心波长处晶体引入的材料二阶色散为61.2 fs^2/mm，三阶色散为39.0 fs^3/mm[23-24]。该锁模状态下谐振腔内色散补偿位置处的三棱镜对间距为620 mm，棱镜插入量为6 mm，在腔内提供的往返二阶色散量约为－1110 fs^2，三阶色散量为－1719 fs^3；空气引入的二阶色散约为20 fs^2/m，三阶色散为10 fs^3/m，可计算得到腔内往返净二阶色散量与三阶色散量分别约为－679 fs^2与－1454 fs^3。腔内存在大量的负色散，容易实现孤子锁模，根据孤子锁模理论可知，锁模脉冲宽度会进一步缩短，导致锁模脉冲宽度变大。如表1所示，相较于文献[15]的结果，该实验获得的脉冲宽度更窄，锁模光谱更宽；相较于文献[16]的结果，该实验获得的锁模平均功率更高。下一步会通过优化腔结构，减小损耗，提高输出功率，提高激光器转化效率，同时更换腔内色散补偿器件，合理精确地控制腔内净色散，期望获得高功率、高转化效率的超短脉冲输出。

表1 绿光泵浦翠绿宝石锁模激光器的性能对比

Table 1 Performance comparison of mode-locked alexandrite lasers pumped by green laser

Pump wavelength / nm	Mode-locked method	Average power / mW	Center wavelength / nm	Spectral width / nm	Pulse width / fs	Frequency / MHz	Year	Institution
532	Kerr-lens mode locking	780	755	3.6	170	80	2016	University of Manitoba, Canada
532	InP/InGaP quantum-dot saturable absorber mode locking	295	755	1.8	380	79.9	2018	University of Manitoba, Canada
532	Kerr-lens mode locking	4	750	9	70	5.6	2018	Koç University, Turkey
532	Graphene saturable absorber mode locking	8	750	9	65	5.56	2018	Koç University, Turkey
532	Kerr-lens mode locking	369	749	6.3	86	92	2023	Xidian University, China

4 结 论

目前，国内在翠绿宝石全固态克尔透镜锁模振荡器方面的研究还处于初步探索阶段，与国际先进的成果还有一定的差距。翠绿宝石晶体的上能级寿命大，容易产生自调Q脉冲，不易产生克尔透镜锁模脉冲，锁模阈值高。我们借鉴国际相关研究方向的研究方法与理论，成功实现了绿光泵浦的翠绿宝石克尔透镜锁模运转，输出平均功率为369 mW，脉冲宽度为86 fs，重复频率为92 MHz，中心波长为749 nm，光谱半峰全宽为6.3 nm。同时，翠绿宝石晶体的发射谱宽在理论上可以支持脉冲宽度小于20 fs的脉冲输出。后续希望通过优化腔参数，并进一步管理腔内色散，获得更好的实验结果，从而可以在未来服务于工业加工、医学美容、通信探测等。

参 考 文 献

[1] 于潇涵，亓东锋，周文举，等. 超快激光制备硫系玻璃表面周期性纳米结构[J]. 激光与光电子学进展，2022，59(15)：1516019.
Yu X H, Qi D F, Zhou W J, et al. Fabrication of periodic nanostructures on the surface of chalcogenide glass using ultrafast laser[J]. Laser & Optoelectronics Progress, 2022, 59(15): 1516019.

[2] 马玉龙，明兴祖，贾松权，等. 飞秒激光加工面齿轮表面的能量耦合模型与齿面形貌研究[J]. 激光与光电子学进展，2022，59(7)：0714009.
Ma Y L, Ming X Z, Jia S Q, et al. Study on energy coupling model and tooth surface morphology of face gear surface machined by femtosecond laser[J]. Laser & Optoelectronics Progress, 2022, 59(7): 0714009.

[3] 宋紫燕，黄俊，李英哲，等. 飞秒激光焊接离体皮肤组织工艺与性能试验研究[J]. 中国激光，2022，49(20)：2007107.
Song Z Y, Huang J, Li Y Z, et al. Experimental study on technology and properties of femtosecond laser welding *in vitro* skin tissue[J]. Chinese Journal of Lasers, 2022, 49(20): 2007107.

[4] 王铁军，陈娜，郭豪，等. 飞秒强激光大气遥感新技术的原理和研究进展[J]. 激光与光电子学进展，2022，59(7)：0700001.
Wang T J, Chen N, Guo H, et al. Principle and research progress of atmospheric remote sensing by intense femtosecond lasers[J]. Laser & Optoelectronics Progress, 2022, 59(7): 0700001.

[5] Liu L J, Liu W, Ji G, et al. NIR emission nanoparticles based on FRET composed of AIE luminogens and NIR dyes for two-photon fluorescence imaging[J]. Chinese Journal of Polymer Science, 2019, 37(4): 401-408.

[6] Jeong T M, Lee J. Generation of high-intensity laser pulses and their applications[M]//Viskup R. High energy and short pulse lasers. London: InTech, 2016.

[7] Peng X Y, Marrakchi A, Walling J C, et al. Watt-level red and UV output from a CW diode array-pumped tunable alexandrite laser [C]//Conference on Lasers and Electro-Optics 2005, May 22-27, 2005, Baltimore, Maryland, United States. Washington, D.C.: Optica Publishing Group, 2005: CMAA5.

[8] Popescu D P, Choo-Smith L P, Flueraru C, et al. Optical coherence tomography: fundamental principles, instrumental designs and biomedical applications[J]. Biophysical Reviews, 2011, 3(3): 155-169.

[9] Fibrich M, Šulc J, Vyhlídal D, et al. Alexandrite spectroscopic and laser characteristic investigation within a 78–400 K temperature range[J]. Laser Physics, 2017, 27(11): 115801.

[10] Loiko P, Ghanbari S, Matrosov V, et al. Dispersion and anisotropy of thermo-optical properties of Alexandrite laser crystal [J]. Optical Materials Express, 2018, 8(10): 3000-3006.

[11] Ghanbari S, Major A. High power continuous-wave Alexandrite laser with green pump[J]. Laser Physics, 2016, 26(7): 075001.

[12] Yorulmaz I, Beyatli E, Kurt A, et al. Efficient and low-threshold Alexandrite laser pumped by a single-mode diode[J]. Optical Materials Express, 2014, 4(4): 776-789.
[13] Demirbas U, Kärtner F X. Alexandrite: an attractive thin-disk laser material alternative to Yb: YAG?[J]. Journal of the Optical Society of America B, 2020, 37(2): 459-472.
[14] Pestryakov E V, Alimpiev A I, Matrosov V N. Prospects for the development of femtosecond laser systems based on beryllium aluminate crystals doped with chromium and titanium ions[J]. Quantum Electronics, 2001, 31(8): 689-696.
[15] Ghanbari S, Akbari R, Major A. Femtosecond Kerr-lens mode-locked Alexandrite laser[J]. Optics Express, 2016, 24(13): 14836-14840.
[16] Ghanbari S, Fedorova K A, Krysa A B, et al. Femtosecond Alexandrite laser passively mode-locked by an InP/InGaP quantum-dot saturable absorber[J]. Optics Letters, 2018, 43(2): 232-234.
[17] Cihan C, Muti A, Baylam I, et al. 70 femtosecond Kerr-lens mode-locked multipass-cavity Alexandrite laser[J]. Optics Letters, 2018, 43(6): 1315-1318.
[18] Cihan C, Kocabas C, Demirbas U, et al. Graphene mode-locked femtosecond Alexandrite laser[J]. Optics Letters, 2018, 43(16): 3969-3972.
[19] Miao R L, Nie Y, Wang S W, et al. Self-mode-locked alexandrite femtosecond lasers with multi-GHz repetition rates[J]. Optics Letters, 2021, 46(8): 1979-1982.
[20] Hu S, Yang C S, Chang S L, et al. Efficacy and safety of the picosecond 755-nm alexandrite laser for treatment of dermal pigmentation in Asians: a retrospective study[J]. Lasers in Medical Science, 2020, 35(6): 1377-1383.
[21] 王英, 汪倩, 鲜燕, 等. 翠绿宝石皮秒激光与Q开关翠绿宝石纳秒激光治疗面部雀斑疗效对比[J]. 中国美容医学, 2019, 28(10): 72-74.
Wang Y, Wang Q, Xian Y, et al. A comparison of the picosecond alexandrite laser and nanosecond alexandrite laser in the treatment of facial freckles[J]. Chinese Journal of Aesthetic Medicine, 2019, 28(10): 72-74.
[22] 丁佐国, 赵艳霞, 冒进成, 等. 皮秒翠绿宝石激光与Q开关翠绿宝石激光治疗太田痣疗效比较[J]. 中国美容医学, 2021, 30(3): 30-33.
Ding Z G, Zhao Y X, Mao J C, et al. Comparison of the efficacy of picosecond alexandrite laser and Q-switched alexandrite laser for treating ota nevus[J]. Chinese Journal of Aesthetic Medicine, 2021, 30(3): 30-33.
[23] Loiko P, Major A. Dispersive properties of alexandrite and beryllium hexaaluminate crystals[J]. Optical Materials Express, 2016, 6(7): 2177-2183.
[24] Walling J, Peterson O, Jenssen H, et al. Tunable alexandrite lasers[J]. IEEE Journal of Quantum Electronics, 1980, 16(12): 1302-1315.

Green-Pumped Kerr-Lens Mode-Locked Alexandrite Laser

Yang Yunxiao[1,4], Yu Yang[2], Tian Wenlong[1*], Zhu Jiangfeng[1**], Wei Zhiyi[3]

[1]*School of Optoelectronic Engineering, Xidian University, Xi'an* 710071, *Shaanxi, China*;
[2]*Academy of Advanced Interdisciplinary Research, Xidian University, Xi'an* 710071, *Shaanxi, China*;
[3]*Beijing National Laboratory for Condensed Matter Physics, Institute of Physics, Chinese Academy of Sciences, Beijing* 100190, *China*;
[4]*China Jiangnan Space Industry Company Group, Guiyang* 550009, *Guizhou, China*

Abstract

Objective A green-pumped Kerr lens mode-locked alexandrite laser is reported. A commercial 532-nm solid-state laser is used as the pump source for the alexandrite laser. Utilizing the pump power of 10 W, stable mode-locked operation at a repetition rate of 92 MHz, with an average power of 369 mW, is obtained. In this case, the pulse width is 86 fs, center wavelength is 749 nm, and full width at half maximum is 6.3 nm.

Methods The alexandrite crystal with a length of 3 mm and doping atomic fraction of 0.22% was selected as the gain medium in the experiment. Given that the pump laser was linearly polarized, the crystal was cut at the Brewster angle and clamped onto a copper heat sink that could pass through the circulating water. To test the conversion efficiency of continuous waves, we measured the continuous-wave output power using coupling output mirrors (OCs) with different transmissivities. Then, we conducted an experimental study on Kerr lens mode locking using an OC with 2% transmissivity. The mode-locking operation was realized by adjusting concave mirror M2 to find a suitable mode-locked position and by appropriately changing the insertion of prism P2.

Results and Discussions When we explore the characteristics of the continuous wave, we obtain the continuous-wave output power curves for different pump powers, as shown in Fig. 2(a). Among them, the highest continuous-wave output power of 1.33 W is realized by an OC with 2% transmissivity, and the output power threshold is 0.37 W, corresponding to a slope efficiency of 14.3%. The highest continuous-wave output powers of 918 mW and 1.03 W are obtained using OCs with 1% and 3% transmissivities, respectively. Furthermore, the output power thresholds are 0.42 W and 2.38 W, corresponding to slope efficiencies of 9.7% and 14.4%, respectively. Additionally, we use an output coupling mirror with 2% transmissivity to examine alexandrite laser Kerr lens mode-locking. Utilizing the pump power of 10 W, the stable mode-locked operation at a repetition rate of 92 MHz, with an average power of 369 mW, is obtained. The mode-locked spectrum of the laser oscillator is measured using a spectrometer, and the results are shown in Fig. 3(a). The center wavelength of the mode-locked spectrum is 748 nm, and the spectral full width at half maximum (FWHM) is 6.3 nm. The pulse width of the mode-locked pulse is 86 fs, which is measured using a commercial autocorrelator as shown in Fig. 3(c).

The Fourier-transform-limited pulse width is calculated based on the optical spectra obtained from the measurements and differs from the pulse width fitted by the measurements, which indicates that the mode-locked pulse output from the oscillator has a certain amount of chirp. The central wavelength of the mode-locked spectrum obtained by the experiment is 748 nm, and the incident polarization direction of the pump light is parallel to the b axis. The second-order dispersion of the alexandrite crystal at the center wavelength is 61.2 fs^2/mm, and the third-order dispersion is 39.0 fs^3/mm. The spacing of the prism pair at the dispersion compensation position in the resonant cavity in this mode-locked state is 620 mm, and the prism insertion is 6 mm, which provides round-trip second-order dispersion of approximately -1110 fs^2 and third-order dispersion of -1719 fs^3 in the cavity. The second-order dispersion introduced by air is approximately 20 fs^2/m, and the third-order dispersion is 10 fs^3/m. Hence, the net round-trip second-order dispersion and third-order dispersion in the cavity are approximately calculated to be -679 fs^2 and -1454 fs^3, respectively. A significant level of negative dispersion exists in the cavity, which makes it easier to realize soliton mode-locking. However, this results in a larger pulse width.

Conclusions Currently, domestic research on the all-solid-state Kerr lens mode-locking oscillator of alexandrite is still in the preliminary exploration stage, and there remains a gap in the advanced results reported globally. Moreover, the large fluorescence lifetime of the alexandrite crystal can easily generate self-tuning Q pulses, making it difficult to establish a Kerr lens mode-locking pulse, and the mode-locking threshold is high. By leveraging international research methods and theories, we successfully realize a Kerr lens mode-locked operation with green light pumping. This operation exhibits an average output power of 369 mW, pulse width of 86 fs, repetition frequency of 92 MHz, center wavelength of 749 nm, and full width at half maximum of 6.3 nm. The alexandrite crystal emission spectral width supports a pulse output with pulse width of less than 20 fs.

Key words lasers; all-solid-state lasers; green laser pumping; Kerr-lens mode-locking; alexandrite